

3D Cal: An Open-Source Software Library for Calibrating Tactile Sensors

Rohan Kota, Kaival Shah, J. Edward Colgate, Gregory Reardon

Abstract—Tactile sensing plays a key role in enabling dexterous and reliable robotic manipulation, but realizing this capability requires substantial calibration to convert raw sensor readings into physically meaningful quantities. Despite its near-universal necessity, the calibration process remains ad hoc and labor-intensive. Here, we introduce 3D Cal, an open-source library that transforms a low-cost 3D printer into an automated probing device capable of generating large volumes of labeled training data for tactile sensor calibration. We demonstrate the utility of 3D Cal by calibrating two commercially available vision-based tactile sensors, DIGIT and GelSight Mini, to reconstruct high-quality depth maps using the collected data and a custom convolutional neural network. In addition, we perform a data ablation study to determine how much data is needed for accurate calibration, providing practical guidelines for researchers working with these specific sensors, and we benchmark the trained models on previously unseen objects to evaluate calibration accuracy and generalization performance. By automating tactile sensor calibration, 3D Cal can accelerate tactile sensing research, simplify sensor deployment, and promote the practical integration of tactile sensing in robotic platforms.

I. INTRODUCTION

TACTILE sensors capture detailed information about contact forces [1], [2] and surface deformations [3]–[5], which has been used to improve robot control [6]–[10], increase haptic transparency in teleoperation [11], [12], support medical diagnostics [13], [14], and even assess the ripeness of fruit [15]. In contrast to vision and audition, which rely on mature and standardized sensing technologies, tactile sensing is still a nascent field encompassing diverse transduction mechanisms—including capacitive [16], resistive [1], magnetic [17], acoustic [18], and vision-based methods [3]–[5]. Deploying tactile sensors often requires expertise in electronics, materials fabrication, and software development, creating significant barriers to adoption for researchers in adjacent disciplines.

To reduce these barriers, researchers have introduced open-source tactile sensor designs with detailed fabrication documentation [19]–[24], and commercial devices such as the GelSight Mini and DIGIT have made high-resolution tactile sensing more affordable and widely available. These hardware

efforts have been complemented by open-source software libraries that offer unified interfaces for tactile sensors [25] and provide simulation environments to model tactile interactions [26]. Together, these initiatives have begun to foster an ecosystem to support and accelerate tactile sensor research and integration across disciplines. Despite these available resources, sensor calibration—an often essential step for converting raw sensor data into physically meaningful quantities such as contact force or surface geometry—has received little attention.

For some transduction mechanisms, such as resistance- or capacitance-based sensors, mapping from raw sensor signals to a target physical quantity is relatively straightforward and can often be approximated using linear or quadratic functions applied to low-dimensional signals (e.g., voltage) to infer quantities like force [27], [28]. In contrast, other sensing modalities, such as vision-based tactile sensors, produce high-dimensional outputs by leveraging the dense data capture of well-established camera technologies [29]. Learning a mapping from this high-dimensional space to either low-dimensional (e.g., force [5], [30], [31]) or other high-dimensional representations (e.g., depth maps [3]–[5], [31], [32]) poses significant challenges. To address the problem, researchers have relied on simplifying assumptions, such as uniform sensor response [33] or negligible cross-talk between sensing regions [28]. However, these assumptions often impose strict fabrication constraints [28], [33] or limit the validity of the calibration to narrow operating regimes (e.g., small displacement ranges [31]). When these assumptions do not hold, many researchers turn to neural networks to learn the complex mappings directly. While effective, these data-driven approaches often require large, labeled datasets [30], [31], [34].

Collecting these datasets is labor-intensive and time-consuming, limiting the practical use of low-cost devices such as DIGIT [19] that were designed to democratize tactile sensing. To alleviate the manual workload, several authors have developed automated procedures to calibrate their sensors. Many of these automated approaches rely on costly hardware that require extensive setup and technical expertise, including industrial 6-DoF robot arms [30], CNC machines [34], or motion-capture systems [31]. These systems also require spatial calibration to align the probing device’s coordinate frame with the sensor, which further complicates the measurement procedure. This limits accessibility for those developing new, experimental sensors or seeking to integrate tactile sensing into broader research workflows with minimal overhead.

This work was supported by the National Science Foundation under Grant NRI-2221571 and HAND ERC 2330040. (Corresponding authors: J. Edward Colgate; Gregory Reardon)

Rohan Kota, Kaival Shah, J. Edward Colgate, and Gregory Reardon are with the Department of Mechanical Engineering, Northwestern University, Evanston, IL 60208 USA.

<rohankota2026, kaivalshah2028>@u.northwestern.edu,
<colgate, gregory.reardon>@northwestern.edu

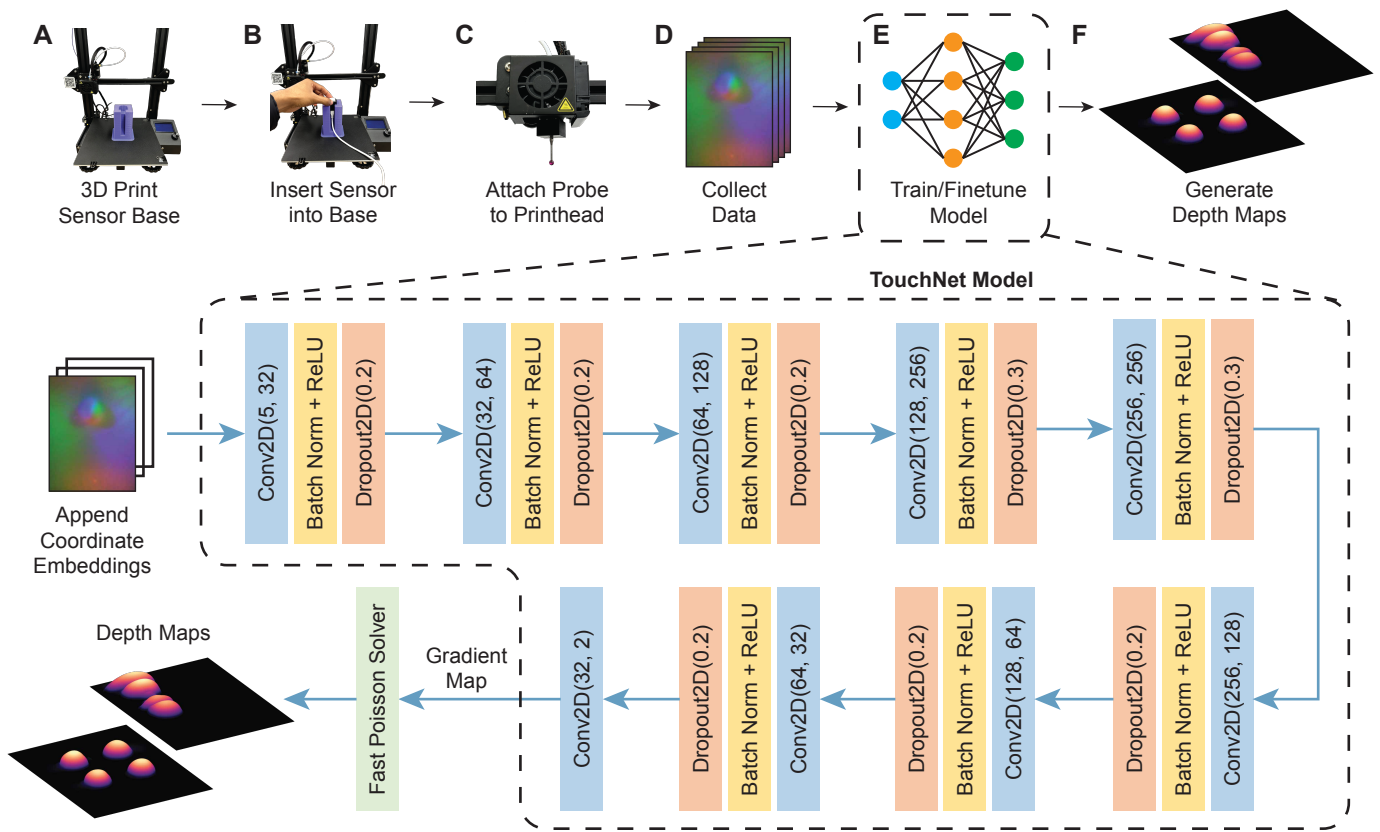


Fig. 1: **Overview of 3D Cal library.** (A) Users first 3D print a sensor base on the print bed. (B) The tactile sensor is then inserted into the base with a slide fit. (C) Next, the 3D printer nozzle is affixed with a probe tip. (D) An automated program then uses the 3D printer to probe the sensor and collect labeled calibration data. (E) The calibration data is then used to train or fine-tune a machine learning model. For vision-based tactile sensors, we include our TouchNet model, which employs a 9-layer convolutional architecture to convert an RGB image, appended with a 2-channel x, y coordinate embedding, into a surface gradient map. (F) The trained models are then used to predict calibration targets, which for TouchNet is an indentation depth map.

Here, we present 3D Cal: an open-source Python library for calibrating tactile sensors by repurposing low-cost Fused Deposition Modelling (FDM) 3D printers into fully automated probing devices to facilitate the rapid capture of large amounts of labeled training data. The 3D printer is first used to print a sensor base, thereby constraining the sensor position within the printer’s workspace, and is then repurposed into a 2-axis gantry that can be easily controlled via G-code to probe the sensor thousands of times. We demonstrate the utility of 3D Cal by using our library to capture thousands of calibration images from two commercial vision-based tactile sensors: the DIGIT and GelSight Mini. We then use this data to train a lightweight network, TouchNet, to generate high-resolution depth maps. Further, we perform an ablation study to determine the quantity of data required to accurately calibrate these two common sensors and benchmark model performance on a set of 3D printed objects with known geometries.

The functionalities provided by 3D Cal are intended to improve the accessibility of tactile sensors through a simple, easy-to-use library that allows roboticists and those in adjacent disciplines such as haptics, human-computer interaction, and medical diagnostics to calibrate tactile sensors for use in their research. We also intend for 3D Cal to accelerate the development of tactile sensors and their associated learning algorithms through large-scale data capture and open-sourcing

of tactile images. Our primary contributions thus include:

- **3D Cal: an open-source Python library** that transforms off-the-shelf 3D printers into fully automated calibration devices for tactile sensors.
- **TouchNet**, a lightweight convolutional neural network for generating depth maps from vision-based tactile sensors, along with automated pipelines to train the model.
- **Practical training data guidelines** for producing high-quality depth maps with the DIGIT and GelSight Mini.

We invite contributions from the community to extend library functionality and support for additional sensors. All software, pre-trained models, and datasets can be found on our project page: <https://rohankotanu.github.io/3DCal>.

II. 3D CAL

3D Cal facilitates the calibration of tactile sensors so that they can be more easily incorporated into research applications. The library provides two main functionalities. First, it streamlines the collection and annotation of data needed to calibrate the sensor (Fig. 1A, B, C, D). Second, it provides software to train machine learning models (Fig. 1E, F). In its current form, model training and inference is limited to vision-based tactile sensing (i.e., RGB image inputs) and the generation of sensor depth maps, though we plan to expand

the functionality to incorporate a wide range of sensors and inference targets.

A. Data Collection

The 3D Cal library makes it easy to collect thousands of calibration measurements from a tactile sensor with minimal user intervention. First, the user designs and 3D-prints a base for their tactile sensor (Fig. 1A), ensuring the sensor can be inserted with a slide fit. Here, because we leverage the 3D printer to print a sensor base, the sensor location is implicitly defined within the printer’s coordinate system. After inserting the sensor into the printed base (Fig. 1B), a probe is mounted to the printhead using a 3D printed adapter (Fig. 1C). We use a rigid, spherical probe tip with a 2 mm radius (McMaster-Carr part no. 85175A586), though users are free to incorporate probe tips of varying size, shape, and material properties. Users then specify the desired probing coordinates (x, y) and depths (z) in a CSV file, and 3D Cal parses the file and probes the sensor accordingly, generating coordinate-labeled training data.

3D Printer Abstraction. 3D Cal is designed to work with any G-Code compatible FDM 3D printer. Our implementation currently supports the Ender 3 (Shenzhen Creality 3D Technology Co, Ltd., Hong Kong), though other 3D printers can be added with only a few lines of additional code because the G-Code commands used in the library are printer-agnostic.

Sensor Abstraction. 3D Cal can be used with any tactile sensor that is planar or has a small radius of curvature. The library is currently optimized to capture data from vision-based tactile sensors, providing built-in support for the DIGIT, GelSight Mini, and any sensor compatible with OpenCV. For custom vision-based tactile sensors, users only need to implement functions to establish sensor communication and acquire images. These functions are invoked by the calibration procedure to automatically connect to the tactile sensor and capture images at the specified probing locations. We provide full data collection support for the DIGIT and GelSight Mini, including sensor base designs, CSV files for probing (0.5 mm \times 0.5 mm grid), and sensor image capture during probing.

B. Model Training

Given the varied transduction principles and calibration targets of different tactile sensors, model training tends to be highly idiosyncratic and thus challenging to design a general-purpose solution for sensor calibration. However, 3D Cal comes with expansive support for training machine learning models to produce depth maps for vision-based tactile sensors (Fig. 1E, F). We targeted this setting first because vision-based tactile sensing is a rapidly expanding and rich research area [35], [36] and the DIGIT and GelSight Mini have a large userbase, are available for consumer purchase, and lack support for automated calibration. These sensors are both available in markerless variants and are optimized for capturing surface geometry during contact, rather than shear forces, making depth prediction a well-aligned and practical calibration objective [35].

TouchNet. To extract meaningful depth information from vision-based tactile sensors, we propose TouchNet, a fully convolutional neural network [37] that maps RGB sensor images to a surface gradient map (Fig. 1E). The input to TouchNet is a 5-channel image: a standard 3-channel RGB image concatenated with a 2-channel positional embedding (x, y coordinate embedding [38]). TouchNet is composed of a feedforward convolutional neural network with 9 sequential modules, each including a convolutional layer, batch normalization [39], a ReLU activation [40], and spatial dropout for regularization [41]. The network begins by expanding the input feature dimensionality from 5 to 256 channels using a sequence of convolutional layers, and then reduces it to 2 output channels representing the predicted surface gradients in the x - and y -directions (G_x, G_y). We found that convolutional architectures with relatively small kernel sizes generalized better to unseen shapes—even when trained only on spherical probes—as they more directly map a set of (R, G, B, x, y) values to a surface gradient (G_x, G_y) , unlike encoder–decoder models such as U-Net, which compress the image into a low-dimensional latent representation.

TouchNet gradient maps are then integrated via a fast Poisson method to yield depth maps (Fig. 1F). 3D Cal enables researchers to either train TouchNet models from scratch or fine-tune them using pre-trained weights from our DIGIT or GelSight Mini models (see Sec. III). The software architecture also allows researchers to quickly design and train new model architectures if desired. In practice, TouchNet inference runs in under 30 ms on modest laptop-grade hardware, enabling real-time depth map generation at 30 fps, which aligns with the typical operating frame rate of many vision-based tactile sensors. As part of 3D Cal, we release our TouchNet architecture, pre-trained weights for our DIGIT and the GelSight Mini, and the calibration image datasets used for training.

III. CALIBRATING COMMERCIAL SENSORS WITH 3D CAL

3D Cal makes it easy to rapidly capture labeled training data and subsequently train machine learning models to predict calibration targets for tactile sensors. In this section, we use 3D Cal to calibrate two commercial sensors, DIGIT and GelSight Mini, to generate high-resolution depth maps. We then use the library to perform ablation studies to determine the quantity of training data required to accurately calibrate these sensors, providing concrete guidelines for individuals who wish to incorporate these sensors into their research.

For the DIGIT and GelSight Mini, we designed and 3D printed a sensor holder (Fig. 1A), attached a spherical probe tip to the printhead (Fig. 1C), and probed along a 0.5 mm \times 0.5 mm grid (Fig. 2A, $d = 0.5$ mm), resulting in a total of 1,221 and 1,209 distinct probe locations, respectively. At each probe location, we captured 30 images during each indentation of the probe sphere (Fig. 1D). Data capture took around 2 hours for each sensor.

All TouchNet models were trained with this data (and varying subsets of this data) using a mean squared error (MSE) loss, an AdamW optimizer with a learning rate of $1e-4$ and weight decay of $1e-4$, and a batch size of 64. Training

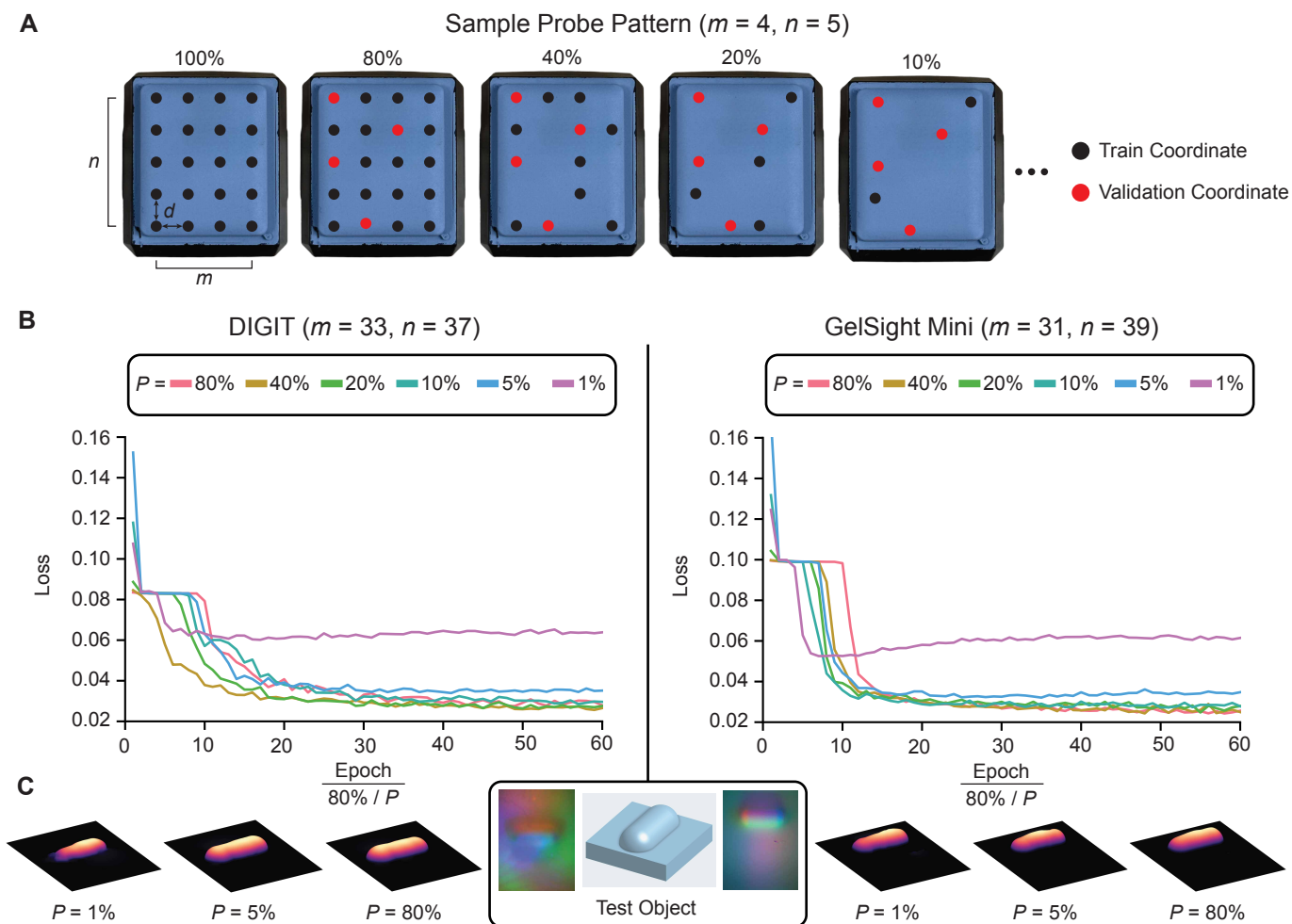


Fig. 2: Results of training data ablation study. (A) Sensors were probed along an $m \times n$ grid with $d = 0.5$ mm spacing. 20% of the coordinates were reserved for validation (red dots) while the remaining coordinates were used for training (black dots). Models were trained on $P = 80\%, 40\%, 20\%, 10\%, 5\%$, and 1% of the total coordinates. (B) Model loss when trained on different percentages, P , of the probed coordinates. To account for differences in the number of batches per epoch, models were trained for $N = 60 \times (\frac{80\%}{P})$ epochs. (C) Reconstructed depth maps (pill-shaped test object) for models trained on different percentages, P , of total coordinates.

was performed in PyTorch on an RTX 6000 GPU (NVIDIA, Santa Clara, CA, USA) using autocast for mixed precision and GradScaler to ensure numerical stability. Models were trained and evaluated on the probe data and later tested on unseen, non-spherical objects.

A. Spatial Sampling Analysis

Owing to non-uniform illumination, vision-based tactile sensors often need to be calibrated at several points across the sensing surface [4], [32]. To determine how densely the sensor surface needed to be sampled, we trained a TouchNet model using randomly selected subsets comprising $P = 80\%, 40\%, 20\%, 10\%, 5\%$, and 1% of the total spatial coordinates present in our dataset. When training the model on 80% of the coordinates, the remaining 20% of coordinates were set aside for validation, and this same validation set was used to evaluate all subsequent models (Fig. 2A). To account for differences in the number of batches per epoch, models were trained for $N = 60 \times (\frac{80\%}{P})$ epochs.

For both the DIGIT (Fig. 2B, left panel) and GelSight Mini (Fig. 2B, right panel), model performance suffered when

trained on 1% of the captured data (12 spatial coordinates), but performed relatively consistently when trained on $\geq 5\%$ of the total data (≥ 61 and 60 spatial coordinates, respectively). This was also reflected in the reconstructed depth maps of a pill-shaped test object (Fig. 2C), which remained visually similar for models trained on 5% and 80% of the coordinates, but deteriorated for the $P = 1\%$ model.

To better understand how the spatial distribution of probing locations affected model performance across the sensing surface, we computed the MSE of the gradient predictions at each probe coordinate in the validation set (Fig. 3A). We restricted our analysis to images where the center of the probe fell within the camera’s field of view (FOV), as some probe locations remained on the gel but were partially or entirely out of the camera’s limited FOV. In regions with sparse training data (Fig. 3A, red X’s), the MSE loss (Fig. 3A, shaded circles) increased markedly, reflecting the non-uniform response of the sensing surface. This was particularly evident for small values of P (e.g., $P = 1\%$). We then approximated the distributions of MSE losses for all values of P using Gaussian

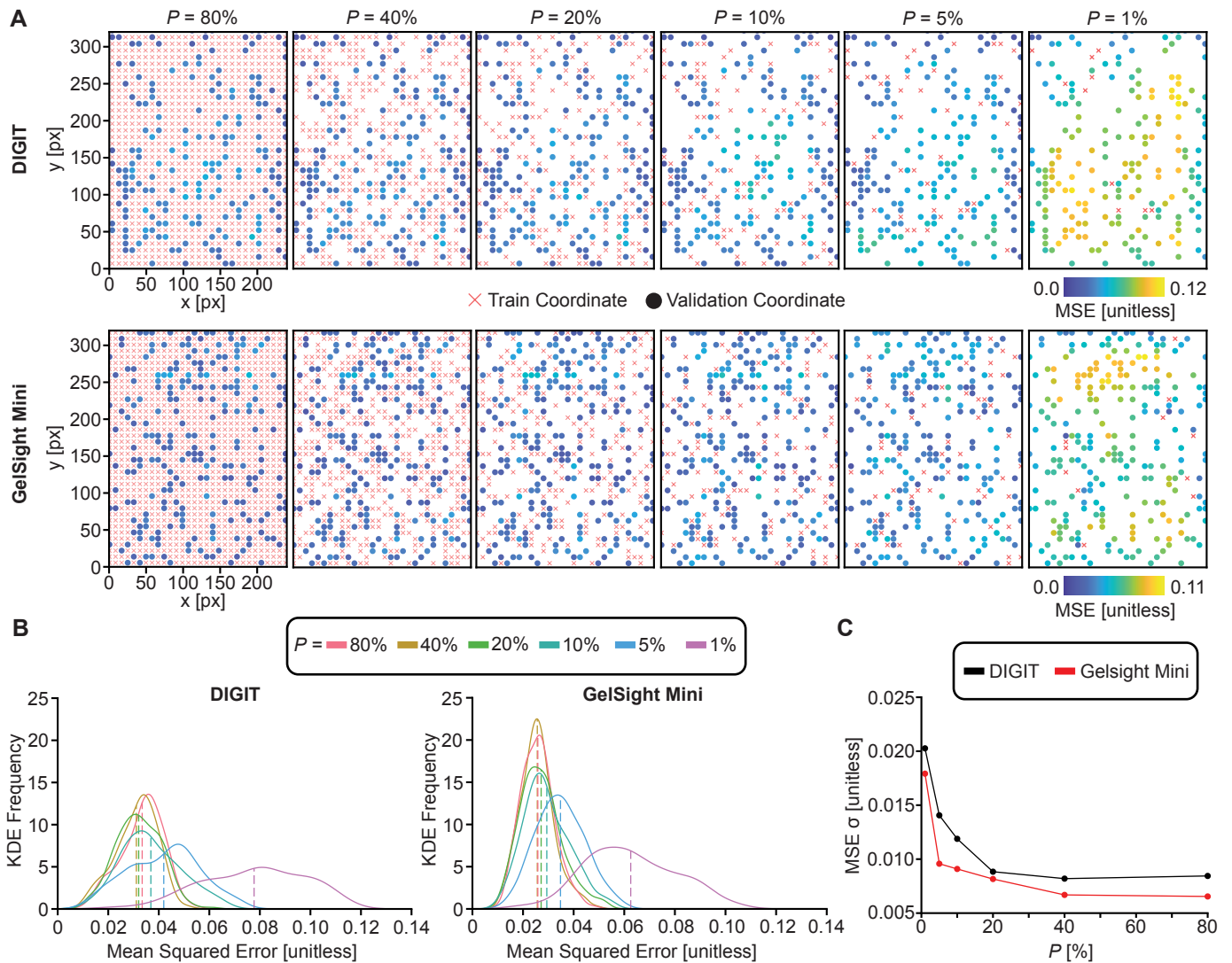


Fig. 3: Spatial distribution of reconstruction accuracy. (A) The mean squared error (MSE) of the output gradients for coordinates in the validation set (shaded circles) using TouchNet models trained on different percentages, P , of the probed coordinates. The MSE tended to be higher in regions with fewer training coordinates (red X's). (B) Kernel density estimates (KDE) of the MSE values (bin width: 0.0015, dashed lines: mean). These distributions tended to converge towards one another for higher values of P . (C) Standard deviation (σ) of MSE distributions for different P values (DIGIT: black line, GelSight Mini: red line).

kernel density estimation (KDE; Fig. 3B). These distributions reveal the spatial variability in reconstruction performance for the spherical calibration object. For both sensors, the average MSE loss (Fig. 3B, dashed lines) and standard deviation of the MSE loss (Fig. 3C) generally decreased as the number of training coordinates increased, suggesting that denser sampling reduced reconstruction variability.

We performed five independent sample t-tests ($\alpha = 0.01$) with a Bonferroni correction to compare the MSE loss distributions of the $P = 40\%$, 20% , 10% , 5% , and 1% models to that of the $P = 80\%$ model. For the DIGIT, the tests revealed a significant difference between the MSE loss distributions of the $P = 80\%$ model compared to the $P = 1\%$ ($t = -27.36$, $p < 0.001$), $P = 5\%$ ($t = -7.06$, $p < 0.001$), and $P = 10\%$ ($t = -3.20$, $p = 0.008$) models. For the GelSight Mini, the tests similarly revealed a significant difference between the MSE loss distributions of the $P = 80\%$ model compared to the $P = 1\%$ ($t = -29.30$, $p < 0.001$), $P = 5\%$ ($t = -11.76$,

$p < 0.001$), and $P = 10\%$ ($t = -4.82$, $p < 0.001$) models. All other t-tests revealed no significant difference compared to the MSE loss distributions of the $P = 80\%$ models. Given the non-parametric shape of the distributions, we also conducted Mann-Whitney U tests and found similar results. Thus, reconstruction performance stabilized when 20% of the coordinates were used to train the model, but further increases in training data yielded negligible improvement. Thus, while cursory evaluation of a single test object revealed reasonable performance even for $P = 5\%$ (Fig. 2C), our evaluations of the validation set suggest that model performance continues to improve with more training data and that it primarily manifests in the form of reduced reconstruction variability across the sensing surface. Consequently, for optimal performance on both sensors, we recommend probing at least 20% of the total coordinates, or approximately 240 randomly selected coordinates along a $0.5 \text{ mm} \times 0.5 \text{ mm}$ grid.

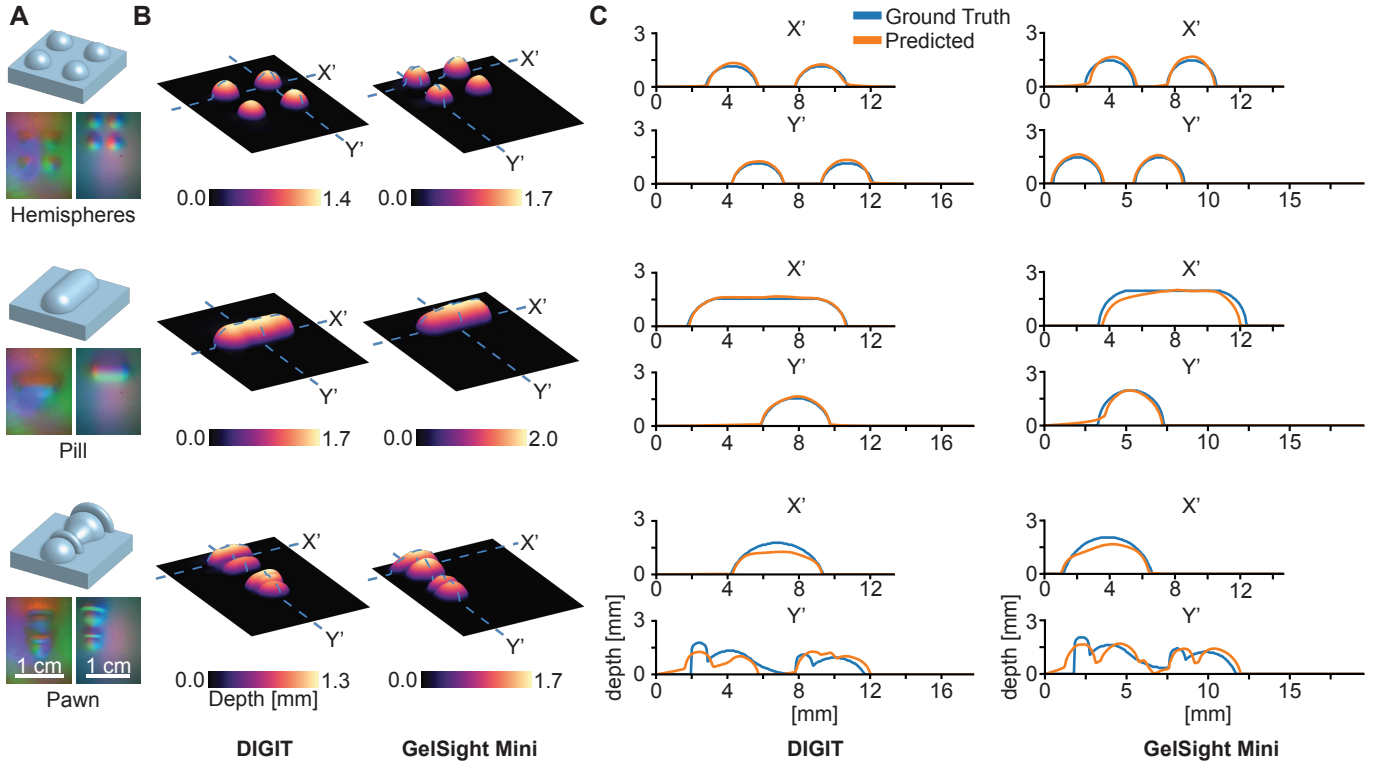


Fig. 4: **Reconstructed depth maps for DIGIT and GelSight Mini using 3D Cal.** (A) Three 3D printed test objects (*hemispheres*, *pill*, *pawn*), all measuring $10\text{ mm} \times 10\text{ mm}$, were pushed into the DIGIT and GelSight Mini. The corresponding RGB images on the DIGIT (bottom left) and GelSight Mini (bottom right) are shown below each test object. (B) The TouchNet models trained on $P = 80\%$ of the probed coordinates were used to predict the depth maps for both sensors. (C) Ground-truth depth maps were computed from the CAD models and a 2D cross-correlation was performed to line up the ground-truth and predicted depth maps. Cross sections along two perpendicular axes show the predicted depth (orange line) relative to the ground-truth depth (blue line).

IV. PERFORMANCE ON UNSEEN OBJECTS

To evaluate our model’s performance on previously unseen objects, we designed 3 test objects in CAD: *hemispheres*, *pill*, and *pawn* (Fig. 4A). The STL representations of these objects were converted into ground-truth depth maps, which served as benchmarks for the depth maps predicted by TouchNet. The objects were 3D printed and manually indented into the sensors, and depth maps were computed using the TouchNet model trained on 80% of the total coordinates (Fig. 4B). Because the indentations were performed manually, the ground-truth depth maps were spatially aligned along the xy -plane using a 2D cross-correlation. To further account for slight variations in indentation depth, the indentation depths of the ground-truth CAD models were adjusted to minimize the mean squared error between the predicted and ground-truth depth maps.

Reconstructed depth maps had a strong visual resemblance to the test object profile (Fig. 4B). To better visualize reconstruction performance, we took representative cross-sections of each depth map (Fig. 4B, dashed lines; Fig. 4C, orange lines) and plotted them against the corresponding ground-truth cross section (Fig. 4C, blue lines). For simpler geometries (e.g., *hemispheres*, *pill*), the DIGIT produced more accurate depth map reconstructions, while the GelSight Mini outperformed DIGIT on the *pawn* (Table I). Notably, both sensors struggled to reconstruct the neck of the pawn-shaped test object, which

was cast in a dark shadow due to the *pawn*’s geometry and the lighting configuration of the sensors (Fig. 4A). In future work, training the model on a more diverse set of probe geometries could enhance its robustness to shadows.

	Test Object	DIGIT [μm]	GelSight Mini [μm]
Overall Error	<i>Hemispheres</i>	16.984	22.413
	<i>Pill</i>	16.274	23.641
	<i>Pawn</i>	52.211	48.821
Type 1 Error	<i>Hemispheres</i>	5.641	5.143
	<i>Pill</i>	8.807	7.557
	<i>Pawn</i>	18.788	17.360
Type 2 Error	<i>Hemispheres</i>	107.127	171.605
	<i>Pill</i>	65.274	152.846
	<i>Pawn</i>	296.381	290.014

TABLE I: Average Overall Error, Type 1 Error, and Type 2 Error for the test object depth maps on the DIGIT and GelSight Mini using TouchNet.

The average reconstruction error across the entire sensing surface ranged from $16.274\ \mu\text{m}$ to $52.211\ \mu\text{m}$ on the DIGIT and $22.172\ \mu\text{m}$ to $48.821\ \mu\text{m}$ on the GelSight Mini (Table I; Overall Error). We then separately analyzed the pixelwise depth errors in regions where the ground-truth depth was zero (Type 1 Errors; Fig. 5A) and non-zero (Type 2 Errors; Fig. 5B). For all three test objects, the average Type 1 error remained

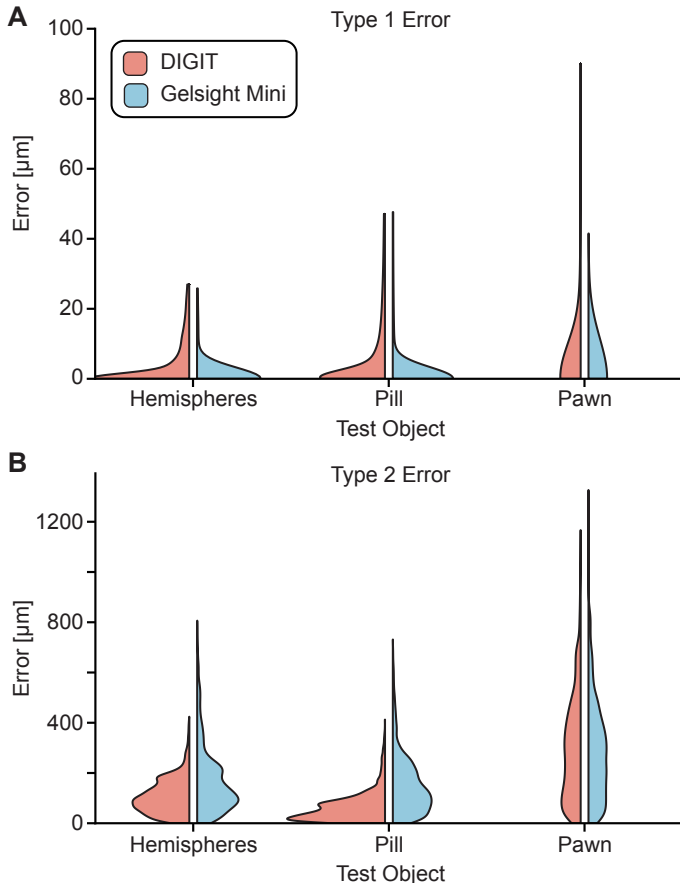


Fig. 5: **Distributions of pixelwise depth map errors.** (A) Violin plots of the pixelwise depth map error distributions where the ground-truth depth was equal to zero (Type 1 Error). Type 1 error distributions were truncated at the 95th percentile for clarity (DIGIT: red, GelSight Mini: blue). (B) Violin plots of the pixelwise depth map error distributions where the ground-truth depth was non-zero (Type 2 Error).

below $20 \mu\text{m}$ for both sensors (Table I, Type 1 Error). Thus, the models were extremely effective at identifying regions on the sensor surface where no contact was occurring. The average Type 2 errors were larger, ranging from $65.274 \mu\text{m}$ to $296.381 \mu\text{m}$ on the DIGIT and $152.846 \mu\text{m}$ to $290.014 \mu\text{m}$ on the GelSight Mini (Table I, Type 2 Error). Although occasional large per-pixel errors occurred in the *pawn* reconstructions, the Type 2 Errors were generally small and concentrated below $200 \mu\text{m}$ for the *hemispheres* and *pill* test objects. Overall, these Type 2 reconstruction errors—approximately 5–15% of the maximum measured indentation depth—are likely suitable for many real-world robotic manipulation tasks.

V. DISCUSSION AND FUTURE WORK

Tactile sensing can enhance robot manipulation and control, as well as enable new research in related domains such as haptics, human-computer interaction, and medical diagnostics. 3D Cal is designed to simplify the deployment of tactile sensors in these settings by streamlining and standardizing the sensor calibration process. By converting low-cost FDM 3D printers into automated probing devices, 3D Cal facilitates large-scale collection of labeled training data for tactile sensors

(Fig. 1). Here, we utilized those capabilities to train a custom convolutional neural network, TouchNet, and generate depth maps for two widely used and commercially available vision-based tactile sensors: DIGIT and GelSight Mini. Our pre-trained model weights will be publicly available, allowing researchers to fine-tune models for their own DIGIT or GelSight Mini, or use 3D Cal to calibrate their sensors from scratch.

We further used 3D Cal to determine the quantity of training data required to accurately calibrate the DIGIT and GelSight Mini. We found that our TouchNet model could generate high-quality depth reconstructions on unseen and complex objects with only moderate amounts of labeled training data from spherical probes (Fig. 4). Further, the spatial variation of reconstruction losses stabilized when the models were trained with data captured from approximately 250 distinct spatial locations across the sensor surface ($P = 20\%$; Fig. 3). These results are consistent with prior work showing that non-uniform illumination in vision-based tactile sensors increases the need for calibration data [4], [32].

While per-sensor calibration is currently the dominant method to generate high-quality tactile measurements, we envision a shift towards transfer learning paradigms [42], [43] and more generalizable, sensor-agnostic models. We believe 3D Cal can help accelerate these efforts through large-scale tactile data capture. To contribute to this goal, and in the spirit of recent research that has released raw tactile images [43]–[46], we also release our dataset of over 70,000 probe images used to train TouchNet.

In future work, we aim to extend 3D Cal to seamlessly interface with force sensors, enabling new calibration targets, such as shear and normal forces. We also plan to enhance our support for capacitance-based, resistance-based, and other emerging tactile sensing technologies. Through these efforts, we hope to lower the barrier to entry for researchers seeking to incorporate tactile sensing into their work, as well as accelerate the development of next-generation tactile sensors and their associated software ecosystems.

ACKNOWLEDGMENTS

This work was made possible by funding from the National Science Foundation Grant No. NRI-2221571 and Grant No. 2330040, the Engineering Research Center (ERC) for Human Augmentation via Dexterity (HAND). The DIGIT sensor used in this research was donated by Meta AI. The authors would also like to thank Andrew Pavlovic for his contributions to this project and Roberto Calandra for his feedback on early iterations of this work.

REFERENCES

- [1] S. Stassi, V. Cauda, G. Canavese, and C. F. Pirri, “Flexible tactile sensing based on piezoresistive composites: A review,” *Sensors*, vol. 14, no. 3, pp. 5296–5332, 2014.
- [2] R. Bhirangi, T. Hellebrekers, C. Majidi, and A. Gupta, “ReSkin: Versatile, replaceable, lasting tactile skins,” in *Conference on Robot Learning (CoRL)*, 2021.
- [3] M. K. Johnson and E. H. Adelson, “Retrographic sensing for the measurement of surface texture and shape,” in *IEEE Conference on Computer Vision and Pattern Recognition*, 2009, pp. 1070–1077.

- [4] M. K. Johnson, F. Cole, A. Raj, and E. H. Adelson, "Microgeometry capture using an elastomeric sensor," *ACM Transactions on Graphics*, vol. 30, no. 4, 2011.
- [5] W. Yuan, S. Dong, and E. H. Adelson, "GelSight: High-resolution robot tactile sensors for estimating geometry and force," *Sensors*, vol. 17, no. 12, 2017.
- [6] R. Calandra, A. Owens, M. Upadhyaya, W. Yuan, J. Lin, E. Adelson, and S. Levine, "The feeling of success: Does touch sensing help predict grasp outcomes?" in *Conference on Robot Learning (CoRL)*, Oct. 2017.
- [7] A. Yamaguchi and C. G. Atkeson, "Combining finger vision and optical tactile sensing: Reducing and handling errors while cutting vegetables," in *2016 IEEE-RAS 16th International Conference on Humanoid Robots*, 2016, pp. 1045–1051.
- [8] T. Bernardi, Y. Fleytoux, J.-B. Mouret, and S. Ivaldi, "Learning height for top-down grasps with the digit sensor," in *2023 IEEE International Conference on Robotics and Automation (ICRA)*, 2023, pp. 1737–1743.
- [9] H. Xu, Y. Luo, S. Wang, T. Darrell, and R. Calandra, "Towards learning to play piano with dexterous hands and touch," in *2022 IEEE/RSJ International Conference on Intelligent Robots and Systems (IROS)*, 2022, pp. 10410–10416.
- [10] P. Sodhi, M. Kaess, M. Mukadam, and S. Anderson, "Patchgraph: In-hand tactile tracking with learned surface normals," in *2022 International Conference on Robotics and Automation (ICRA)*, 2022, pp. 2164–2170.
- [11] M. Lippi, M. C. Welle, M. K. Wozniak, A. Gasparri, and D. Kragic, "Low-cost teleoperation with haptic feedback through vision-based tactile sensors for rigid and soft object manipulation," in *2024 33rd IEEE International Conference on Robot and Human Interactive Communication (ROMAN)*, 2024, pp. 1963–1969.
- [12] G. Giudici, A. A. Bonzini, C. Coppola, K. Althoefer, I. Farkhatdinov, and L. Jamone, "Leveraging tactile sensing to render both haptic feedback and virtual reality 3D object reconstruction in robotic telemanipulation," *arXiv preprint arXiv:2412.02644*, 2024.
- [13] C.-H. Won, J.-H. Lee, and F. Saleheen, "Tactile sensing systems for tumor characterization: A review," *IEEE Sensors Journal*, vol. 21, no. 11, pp. 12578–12588, 2021.
- [14] S.-H. Cho, S.-M. Lee, N.-Y. Lee, B. C. Ko, H. Kim, D.-J. Jang, and J.-H. Lee, "High-resolution tactile-sensation diagnostic imaging system for thyroid cancer," *Sensors*, vol. 23, no. 7, 2023.
- [15] S. Li, W. Sun, Q. Liang, C. Liu, and J. Liu, "Assessing fruit hardness in robot hands using electric gripper actuators with tactile sensors," *Sensors and Actuators A: Physical*, vol. 365, p. 114843, 2024.
- [16] O. Glauser, D. Panozzo, O. Hilliges, and O. Sorkine-Hornung, "Deformation capture via soft and stretchable sensor arrays," *ACM Trans. Graph.*, vol. 38, no. 2, Mar. 2019.
- [17] R. Bhirangi, V. Pattabiraman, E. Erciyes, Y. Cao, T. Hellebrekers, and L. Pinto, "AnySkin: Plug-and-play skin sensing for robotic touch," in *2025 IEEE International Conference on Robotics and Automation (ICRA)*, 2025, pp. 16563–16570.
- [18] M. S. Li and H. S. Stuart, "Acoustac: Tactile sensing with acoustic resonance for electronics-free soft skin," *Soft Robotics*, vol. 12, no. 1, pp. 109–123, 2025.
- [19] M. Lambeta, G. Kammerer, D. Jayaraman, R. Calandra, P.-W. Chou, S. Tian, B. Yang, B. Maloon, V. Most, D. Stroud, R. Santos, and A. Byagowi, "DIGIT: A novel design for a low-cost compact high-resolution tactile sensor with application to in-hand manipulation," *IEEE Robotics and Automation Letters*, vol. 5, no. 3, pp. 3838–3845, Feb. 2020.
- [20] A. Sipos, W. van den Bogert, and N. Fazeli, "GelSlim 4.0: Focusing on touch and reproducibility," *arXiv preprint arXiv:2409.19770*, 2024.
- [21] C. Lin, H. Zhang, J. Xu, L. Wu, and H. Xu, "9DTact: A compact vision-based tactile sensor for accurate 3D shape reconstruction and generalizable 6D force estimation," *arXiv preprint arXiv:2308.14277*, 2023.
- [22] M. Lambeta, T. Wu, A. Sengul, V. R. Most, N. Black, K. Sawyer, R. Mercado, H. Qi, A. Sohn, B. Taylor *et al.*, "Digitizing touch with an artificial multimodal fingertip," *arXiv preprint arXiv:2411.02479*, 2024.
- [23] V. Pattabiraman, Z. Huang, D. Panozzo, D. Zorin, L. Pinto, and R. Bhirangi, "eFlesh: Highly customizable magnetic touch sensing using cut-cell microstructures," *arXiv preprint arXiv:2506.09994*, 2025.
- [24] B. Ward-Cherrier, N. Pestell, L. Cramphorn, B. Winstone, M. Giannaccini, J. Rossiter, and N. Lepora, "The TacTip family: Soft optical tactile sensors with 3D-printed biomimetic morphologies," *Soft Robotics*, vol. 5, Jan. 2018.
- [25] M. Lambeta, H. Xu, J. Xu, P.-W. Chou, S. Wang, T. Darrell, and R. Calandra, "PyTouch: A machine learning library for touch processing," in *2021 IEEE International Conference on Robotics and Automation (ICRA)*, 2021, pp. 13208–13214.
- [26] S. Wang, M. Lambeta, P.-W. Chou, and R. Calandra, "Tacto: A fast, flexible, and open-source simulator for high-resolution vision-based tactile sensors," *IEEE Robotics and Automation Letters*, vol. 7, no. 2, p. 3930–3937, Apr. 2022.
- [27] B. Huang, Y. Wang, X. Yang, Y. Luo, and Y. Li, "3D-ViTac: Learning fine-grained manipulation with visuo-tactile sensing," in *Conference on Robot Learning (CoRL)*, 2024.
- [28] A. Cirillo, P. Cirillo, G. D. Maria, C. Natale, and S. Pirozzi, "Modeling and calibration of a tactile sensor for robust grasping," *IFAC-PapersOnLine*, vol. 50, no. 1, pp. 6843–6850, 2017.
- [29] K. Shimonomura, "Tactile image sensors employing camera: A review," *Sensors*, vol. 19, no. 18, 2019.
- [30] A.-H. Shahidzadeh, G. M. Caddeo, K. Alapati, L. Natale, C. Fermüller, and Y. Aloimonos, "FeelAnyForce: Estimating contact force feedback from tactile sensation for vision-based tactile sensors," in *2025 IEEE International Conference on Robotics and Automation (ICRA)*, 2025, pp. 251–257.
- [31] W. K. Do, M. Strong, A. Swann, B. Lei, and M. K. III, "TensorTouch: Calibration of tactile sensors for high resolution stress tensor and deformation for dexterous manipulation," *arXiv preprint arXiv:2506.08291*, 2025.
- [32] S. Wang, Y. She, B. Romero, and E. Adelson, "GelSight Wedge: Measuring high-resolution 3D contact geometry with a compact robot finger," in *IEEE International Conference on Robotics and Automation (ICRA)*, May 2021, pp. 6468–6475.
- [33] S. Dong, W. Yuan, and E. H. Adelson, "Improved GelSight tactile sensor for measuring geometry and slip," in *2017 IEEE/RSJ International Conference on Intelligent Robots and Systems (IROS)*, 2017, pp. 137–144.
- [34] W. K. Do and M. Kennedy, "DenseTact: Optical tactile sensor for dense shape reconstruction," in *2022 International Conference on Robotics and Automation (ICRA)*, 2022, pp. 6188–6194.
- [35] H. Li, Y. Lin, C. Lu, M. Yang, E. Psomopoulou, and N. F. Lepora, "Classification of vision-based tactile sensors: A review," *IEEE Sensors Journal*, 2025.
- [36] S. Luo, N. F. Lepora, W. Yuan, K. Althoefer, G. Cheng, and R. Dahiya, "Tactile robotics: An outlook," *IEEE Transactions on Robotics*, 2025.
- [37] Y. LeCun, L. Bottou, Y. Bengio, and P. Haffner, "Gradient-based learning applied to document recognition," *Proceedings of the IEEE*, vol. 86, no. 11, pp. 2278–2324, 1998.
- [38] R. Liu, J. Lehman, P. Molino, F. Petroski Such, E. Frank, A. Sergeev, and J. Yosinski, "An intriguing failing of convolutional neural networks and the CoordConv solution," *Advances in Neural Information Processing Systems*, vol. 31, 2018.
- [39] S. Ioffe and C. Szegedy, "Batch normalization: Accelerating deep network training by reducing internal covariate shift," in *Proceedings of the 32nd International Conference on Machine Learning*, vol. 37, Jul. 2015, pp. 448–456.
- [40] A. F. Agarap, "Deep learning using rectified linear units (ReLU)," *arXiv preprint arXiv:1803.08375*, 2019.
- [41] J. Tompson, R. Goroshin, A. Jain, Y. LeCun, and C. Bregler, "Efficient object localization using convolutional networks," pp. 648–656, 2015.
- [42] S. Rodriguez, Y. Dou, M. Oller, A. Owens, and N. Fazeli, "Touch2Touch: Cross-modal tactile generation for object manipulation," *arXiv preprint arXiv:2409.08269*, 2024.
- [43] C. Higuera, A. Sharma, C. K. Bodduluri, T. Fan, P. Lancaster, M. Kalakrishnan, M. Kaess, B. Boots, M. Lambeta, T. Wu *et al.*, "SparsH: Self-supervised touch representations for vision-based tactile sensing," *arXiv preprint arXiv:2410.24090*, 2024.
- [44] S. Suresh, Z. Si, S. Anderson, M. Kaess, and M. Mukadam, "Midastouch: Monte-carlo inference over distributions across sliding touch," in *Conference on Robot Learning (CoRL)*, 2023, pp. 319–331.
- [45] R. Gao, Z. Si, Y.-Y. Chang, S. Clarke, J. Bohg, L. Fei-Fei, W. Yuan, and J. Wu, "Objectfolder 2.0: A multisensory object dataset for sim2real transfer," in *Proceedings of the IEEE/CVF Conference on Computer Vision and Pattern Recognition*, 2022, pp. 10598–10608.
- [46] F. Yang, C. Ma, J. Zhang, J. Zhu, W. Yuan, and A. Owens, "Touch and go: Learning from human-collected vision and touch," in *Proceedings of the 36th International Conference on Neural Information Processing Systems*, 2022.